Ground-state energy of an exciton in a quantum-dot superlattice grown on a terraced substrate

Guy Lamouche and Yves Lépine
Département de Physique et Groupe de Recherche en Physique et Technologie des Couches Minces, Université de Montréal, Case Postale 6128, Succursale Centre-ville, Montréal, Québec, Canada H3C 3J7
(Received 20 December 1995)

For adequate material combinations, the growth of a fractional monolayer on a terraced substrate is expected to form a two-dimensional superlattice of flat square quantum boxes. We present a variational calculation of the ground-state energy of an exciton in such a structure. The treatment is performed within a two-band effective mass approximation. Numerical results are presented for the heavy-hole exciton in an InAs/InP quantum-dot superlattice, giving the exciton ground-state energy, the contribution of the electron-hole interaction to this energy, and the extension of the exciton wave function in the superlattice plane. These calculations indicate that the exciton ground-state energy varies considerably with the quantum-dot superlattice parameters. A fair agreement is found with the few available experimental results. [S0163-1829(96)09231-4]

I. INTRODUCTION

Due to the growing interest in the quantum-dot (QD) structures, many techniques have been proposed for their fabrication. One of them is the growth of a fractional monolayer on a terraced substrate.[1] In this technique, the substrate is slightly inclined during the growth, thus presenting terraces on its surface. The QD material is grown from the step edges of the surface. With the deposition of less than a monolayer of the QD material, one expects the formation a two-dimensional (2D) superlattice of one monolayer thick nanoclusters. Such superlattices have been fabricated with InAs/GaAs (Ref. 1) and InAs/InP (Ref. 2) systems.

For an InAs/GaAs QD superlattice, the optical characterization performed by Brandt *et al.* indicates that the limited lateral extension of the quantum dots does modify the recombination kinetics but does not affect much the exciton ground-state energy.[1] This behavior of the ground-state energy is quite different from the results obtained by Leonelli *et al.* for an InAs/InP QD superlattice.[3] For this system, the optical characterization clearly shows that for a given superlattice period the exciton ground-state energy increases when the lateral dimension of the quantum dots decreases.

In this paper, we present a simple variational treatment for the calculation of the ground-state energy of an exciton in a QD superlattice grown on a terraced substrate. This ground-state energy is the quantity measured by photoluminescence. Our model is an attempt to describe the experimental behavior observed in the InAs/InP system. We thus study the variation of the exciton ground-state energy with the parameters of the superlattice. Our treatment provides an estimate of the lateral extension of the exciton wave function. This is useful for discussing recombination kinetics. Finally, we also analyze the contribution of the electron-hole interaction to the exciton ground-state energy.

In Sec. II, we present the variational formalism used to describe the exciton. The exciton wave function is written in terms of the one-particle electron and hole ground states of the QD superlattice. Those ground states are characterized in Sec. III. The variational expression for the expectation value of the exciton energy is derived in Sec. IV in a form which can be easily handled numerically. Numerical results are presented in Sec. V for the heavy-hole exciton in an InAs/InP QD superlattice and a conclusion follows in Sec. VI. Some details of the calculations of Sec. IV are provided in the Appendix.

II. FORMALISM

The ideal 2D QD superlattice obtained by the growth of a fractional monolayer film on a terraced substrate is depicted in Fig. 1. As a first approximation, we neglect the vertical misalignment of the quantum dots and we consider a periodic distribution of flat square boxes in a plane (the x-y plane) perpendicular to the growth axis (z axis). The period of the superlattice (L) is determined by the orientation of the [001] surface of the substrate which fixes the area of the terraces. The lateral dimension the boxes (L_p) is determined by the coverage factor which is the fraction of the monolayer that is covered with the QD material. The boxes are one monolayer thick. After the creation of the quantum dots, the

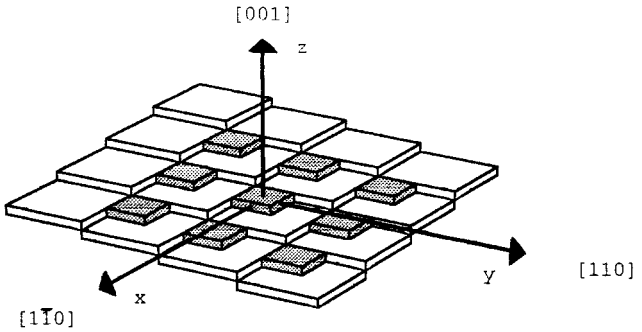

FIG. 1. Vicinal [001] substrate surface tilted slightly towards [100]. It consists of two adjacent staircases with steps running along [110] and [$\bar{1}$10] directions. Shaded boxes represent the clusters grown at the terrace step edges.

substrate material is overgrown. The superlattice is thus embedded in a matrix. We assume that both the substrate and QD material are of zinc-blende structure.

To study the exciton, we rely on a two-band effective-mass approximation. Simple two-band models have been applied to InAs/GaAs (Ref. 4) and InAs/InP (Refs. 3, 5, and 6) thin quantum wells, giving good agreement with experimental optical measurements. We assume that the two bands are isotropic, parabolic, and nondegenerate, the substrate electron and hole effective masses being denoted by m_e^* and m_h^* respectively. In all the equations, the lengths are given in units of a, the substrate lattice constant. The energies are written in units of $\Theta=\hbar^2/(2m_{\rm exc}^* a^2)$, where $m_{\rm exc}^*$ is the substrate exciton effective mass [$m_{\rm exc}^*=1/(1/m_e^*+1/m_h^*)$].

With the origin of the coordinate system at the center of a quantum box, we write the effective Hamiltonian for the exciton as

$$H=-\frac{\nabla_e^2}{\sigma_e}-\frac{\nabla_h^2}{\sigma_h}+V_e(\vec{r}_e)+V_h(\vec{r}_h)-\frac{U}{|\vec{r}_e-\vec{r}_h|}, \qquad (1)$$

where $\sigma_i=m_i^*/m_{\rm exc}^*$ $(i=e,h)$. The last term of Eq. (1) represents the Coulomb interaction with $U=e^2/(\epsilon a\Theta)$, ϵ being the static dielectric constant of the substrate. The functions $V_e(\vec{r}_e)$ and $V_h(\vec{r}_h)$ denote the electron and hole confining potentials introduced by the QD superlattice. We model both potentials with $(i=e,h)$

$$V_i(\vec{r}_i)=-\mathcal{V}_i U_{L_p}(x_i,y_i)\,\delta(z_i), \qquad (2)$$

where $U_{L_p}(x_i,y_i)$ is a periodic function which has a value of unity within the quantum dots and is null elsewhere. Assuming that the exciton wave function is distributed over several lattice sites along the growth direction, it is a good approximation to introduce a δ potential in the z direction since the QD potential is one monolayer thick. For each band, we estimate the amplitude of the potential $(\mathcal{V}_i)$ by multipliying the band offset with the thickness of a monolayer.

Our variational excitonic wave function is

$$\Psi_{\rm exc}(\vec{r}_e,\vec{r}_h)=C\psi_e(\vec{r}_e)\psi_h(\vec{r}_h)F(\vec{r}_e,\vec{r}_h), \qquad (3)$$

where C is a normalization constant and

$$F(\vec{r}_e,\vec{r}_h)=\exp[-\alpha_{xy}\sqrt{(x_e-x_h)^2+(y_e-y_h)^2}], \qquad (4)$$

where α_{xy} is a variational parameter. The functions $\psi_e(\vec{r}_e)$ and $\psi_h(\vec{r}_h)$ are the electron and hole one-particle ground-state wave functions of the superlattice potential. They thus correspond to the Bloch states associated with the extrema of the superlattice electron and hole minibands. They are both obtained from an equation of the form

$$\left[-\frac{\nabla_i^2}{\sigma_i}+V_i(\vec{r}_i)\right]\psi_i(\vec{r}_i)=E_i\psi_i(\vec{r}_i). \qquad (5)$$

In the following, we refer to the absolute value of E_i as the electron or hole confinement energy. Finally, by minimizing the expectation value of the Hamiltonian with respect to α_{xy},

$$E_{\rm exc}(\alpha_{xy})=\frac{\langle\Psi_{\rm exc}(\vec{r}_e,\vec{r}_h)|H|\Psi_{\rm exc}(\vec{r}_e,\vec{r}_h)\rangle}{\langle\Psi_{\rm exc}(\vec{r}_e,\vec{r}_h)|\Psi_{\rm exc}(\vec{r}_e,\vec{r}_h)\rangle}, \qquad (6)$$

we determine the ground-state energy $E_{\rm exc}$ of the exciton and its approximate wave function.

Since we have chosen $F(\vec{r}_e,\vec{r}_h)$ to be independent of z_e and z_h, we assume that the confinement along the growth direction (z axis) is strong enough to neglect the Coulomb correlation induced along that direction. Our variational wave function is based on the one-particle Bloch states corresponding to the extrema of the electron and hole superlattice minibands. We thus expect our variational treatment to be suitable for a superlattice period L smaller than the Coulomb correlation length $1/\alpha_{xy}$ if the superlattice potential weakly modulates the one-particle wave functions. In that case, our treatment can be seen as an effective mass approximation applied to the superlattice structure since (i) the superlattice effective mass of the exciton is similar to that of the substrate, the latter being used in Eq. (6), and (ii) the periodic parts of the electron and hole wave functions do not vary much over a wide range of the Brillouin zone, which is implicitly assumed in our variational wave function. For L larger than $1/\alpha_{xy}$, our formalism should be suitable for a strongly confining potential. That limit corresponds to a quantum-dot array and our variational wave function is then similar to that used for isolated quantum dots.[7,9] Before proceeding to the transformation of Eq. (6) into a form more convenient for numerical evaluation, we characterize the one-particle ground states of the superlattice.

III. THE ONE-PARTICLE GROUND STATES

In this section, we evaluate the electron and hole one-particle ground-state wave functions and the corresponding confinement energies. We solve Eq. (5) in detail for the electron case, the treatment being similar for the hole. Note that, in the following, *the terms ''wave number'' and ''unit cell'' apply to the 2D QD superlattice.*

The electronic ground state lies at the bottom of the lowest superlattice miniband. It is thus characterized by a null wave number in the x-y plane. Due to the symmetry of the potential, the wave function must belong to the representation A_1 of the group D_{4h}. We thus express $\psi_e(\vec{r}_e)$ with the following expansion:

$$\psi_e(\vec{r}_e)=\sum_{n_1\geq n_2} C_{e,n_1,n_2}XY_{n_1,n_2}(x_e,y_e)Z_{e,n_1,n_2}(z_e), \qquad (7)$$

where n_1 and n_2 are zero or positive integers. The basis functions $XY_{n_1,n_2}(x_e,y_e)$ are chosen orthonormal over a unit cell and are given by

$$XY_{n_1,n_2}(x_e,y_e)=N_{n_1,n_2}[\cos(n_1qx_e)\cos(n_2qy_e)+\cos(n_2qx_e)\cos(n_1qy_e)], \qquad (8)$$

with $q=2\pi/L$. The normalization constant is

$$N_{n_1,n_2}=\frac{1}{L}\left[\frac{2}{(1+\delta_{n_1,0})(1+\delta_{n_2,0})(1+\delta_{n_1,n_2})}\right]^{1/2}, \quad (9)$$

where $\delta_{i,j}$ is the Kronecker delta. In Sec. V, we use a limited expansion for Eq. (7). For this purpose, the basis functions will be ordered in ascending order according to the value of $n_1^2+n_2^2$.

To obtain the expansion cofficients C_{e,n_1,n_2} and the z-dependent functions $Z_{e,n_1,n_2}(z_e)$, we substitute $\psi_e(\vec{r}_e)$ into Eq. (5), multiply both sides by $XY_{n_3,n_4}(x_e,y_e)$, and integrate over a unit cell in the x-y plane. This leads to the following system of equations:

$$\left[\frac{(n_3^2+n_4^2)}{\sigma_e}q^2-E_e-\frac{1}{\sigma_e}\frac{d^2}{dz_e^2}\right]C_{e,n_3,n_4}Z_{e,n_3,n_4}(z_e)$$
$$-\mathcal{V}_e\delta(z_e)\sum_{n_1\geq n_2}U_{L_p,n_1,n_2,n_3,n_4}C_{e,n_1,n_2}Z_{e,n_1,n_2}(z_e)=0, \quad (10)$$

where

$$U_{L_p,n_1,n_2,n_3,n_4}=2N_{n_1,n_2}N_{n_3,n_4}[W(n_1,n_3)W(n_2,n_4)+W(n_1,n_4)W(n_2,n_3)], \quad (11)$$

with

$$W(n_1,n_2)=\begin{cases}L_p & \text{if } n_1=n_2=0;\\ \dfrac{\sin(n_1qL_p)}{2n_1q}+\dfrac{L_p}{2} & \text{if } n_1=n_2\neq 0;\\ \dfrac{\sin[(n_1+n_2)qL_p/2]}{(n_1+n_2)q}+\dfrac{\sin[(n_1-n_2)qL_p/2]}{(n_1-n_2)q} & \text{if } n_1\neq n_2.\end{cases} \quad (12)$$

For the ground state, Eq. (10) can only be solved if the functions $Z_{e,n_1,n_2}(z_e)$ do not vanish at the origin. Enforcing that these functions take a value of unity for $z_e=0$, the solutions of Eq. (10) take the form

$$Z_{e,n_1,n_2}(z_e)=\exp(-\beta_{e,n_1,n_2}|z_e|), \quad (13)$$

where

$$\beta_{e,n_1,n_2}=\sqrt{(n_1^2+n_2^2)q^2-E_e\sigma_e}, \quad (14)$$

if the following system of equations is verified:

$$\frac{2}{\sigma_e}\sqrt{(n_3^2+n_4^2)q^2-E_e\sigma_e}C_{e,n_3,n_4}$$
$$-\mathcal{V}_e\sum_{n_1\geq n_2}U_{L_p,n_1,n_2,n_3,n_4}C_{e,n_1,n_2}=0. \quad (15)$$

To obtain the electron confinement energy $|E_e|$ and the expansion coefficients C_{e,n_1,n_2}, we find numerically the lowest value of E_e for which the above system has a nontrivial solution. This also defines the functions $Z_{e,n_1,n_2}(z_e)$. If a similar development is made for the hole, this completes the characterization of the one-particle ground states.

IV. EXCITON GROUND-STATE ENERGY

We now transform the expression for the expectation value of the exciton energy [Eq. (6)] in a form which is suitable for numerical calculations. Using the fact that $\psi_e(\vec{r}_e)$ and $\psi_h(\vec{r}_h)$ are solutions of Eq. (5) with the fact that $F(\vec{r}_e,\vec{r}_h)$ only depends on the relative coordinates of the electron and the hole in the x-y plane, one can find, after simple manipulations including an integration by part,

$$E_{\rm exc}(\alpha_{xy})=E_e+E_h+\alpha_{xy}^2-U\frac{\int_V\int_V\psi_e(\vec{r}_e)^2\psi_h(\vec{r}_h)^2F(\vec{r}_e,\vec{r}_h)^2/|\vec{r}_e-\vec{r}_h|d^3r_ed^3r_h}{\int_V\int_V\psi_e(\vec{r}_e)^2\psi_h(\vec{r}_h)^2F(\vec{r}_e,\vec{r}_h)^2d^3r_ed^3r_h}, \quad (16)$$

where V is the volume of the sample. All the integrals in the x-y plane diverge for a sample that is infinite in this plane. The integrals are thus evaluated on a macroscopic area A.

Both six-dimensional integrals can be reduced to lower dimensional forms. The details of the derivation are sketched in the Appendix and we only give the results here. Our derivation is performed using Fourier expansions. The results are thus given as summations over the reciprocal lattice vectors of the 2D superlattice. As discussed below, for computational purposes, it is better to use expressions where the contributions from the reciprocal lattice vectors with the same norm K_{xy} are combined. We obtain

$$\int_V \int_V \psi_e(\vec{r}_e)^2 \psi_h(\vec{r}_h)^2 F(\vec{r}_e,\vec{r}_h)^2 d^3r_e d^3r_h$$

$$= \frac{\pi A \alpha_{xy}}{16} \sum_{K_{xy}} \frac{M_1(K_{xy})}{(4\alpha_{xy}^2 + K_{xy}^2)^{3/2}} \tag{17}$$

and

$$\int_V \int_V \frac{\psi_e(\vec{r}_e)^2 \psi_h(\vec{r}_h)^2 F(\vec{r}_e,\vec{r}_h)^2}{|\vec{r}_e - \vec{r}_h|} d^3r_e d^3r_h$$

$$= \frac{\pi A}{32} \sum_{K_{xy}} \int_0^\infty e^{-2\alpha_{xy}\rho} \rho J_0(K_{xy}\rho) \int_0^\infty \frac{M_2(K_{xy},w)}{\sqrt{\rho^2+w^2}} dw d\rho, \tag{18}$$

where $J_0(K_{xy}\rho)$ is the zeroth order Bessel function[8] and the functions $M_1(K_{xy})$ and $M_2(K_{xy},w)$ are defined in the Appendix.

Although odd-looking, the resulting expressions constitute a good starting point for the elaboration of a numerical algorithm. Equation (17) can be quickly evaluated for the various values of α_{xy}. The definition of $M_2(K_{xy},w)$ indicates that Eq. (18) involves a summation of two-dimensional integrals. With a good algorithm, one can detect the many terms that are equivalent and thus reduce the number of integrals to perform. The number of terms to include in the summations of Eqs. (17) and (18) is determined by the number of functions used in the expansion of the one-particle wave functions [Eq. (7)]. In practice, as discussed in the following section, one can restrict the summations to the lowest values of K_{xy} and still obtain a very good precision.

V. INAS/INP QUANTUM-DOT SUPERLATTICES

To illustrate the above formalism, we study the heavy-hole exciton in an InAs/InP QD superlattice. Such superlattices have been grown by Tran *et al.*[2] and optically characterized by Leonelli *et al.*[3] In this section, we first provide details on the numerical treatment and we determine the various parameters needed for the calculations. We then proceed to evaluate the exciton ground-state energy for structures of the dimensions reported in Ref. 3. We finally consider QD superlattices of various QD dimensions and periods to get a better picture of the ground-state energy dependence. Note that, in the following, we use the term ''binding energy'' for the magnitude of the ground-state energy of the exciton $|E_{\rm exc}|$. To discuss the influence of the Coulomb interaction, we also introduce the correlation energy $E_{\rm corr} = E_{\rm exc} - E_e - E_h$.[9]

All the numerical calculations presented in this section are performed using 32 basis functions in the expansion of the one-particle wave functions [Eq. (7)]. This choice corresponds to basis functions presenting at most eight oscillations along the x or y direction within a superlattice unit cell. The electron and hole confinement energies are evaluated by finding the lowest value E_i for which the determinant of Eq. (15) vanishes. The coefficients C_{i,n_1,n_2} are then obtained from the null space of the appropriate matrix. In the worst cases, we estimate the numerical precision of the confinement energies to be better than 1%. For all the cases considered, we have verified that the confinement along the growth direction is strong enough to neglect the correlation introduced by the Coulomb interaction along that direction. The use of 32 basis functions implies that 121 values of K_{xy} should be considered in the summations of Eqs. (17) and (18). We have found that restricting the summations to the 5 lowest values of K_{xy} provides a good precision for the correlation energy for all the superlattices studied here, thus reducing considerably the computing time. In all the figures, the symbols represent the calculated values, while the lines have been added as a guide.

TABLE I. Material parameters. The values are taken from Ref. 14, except for the InP heavy-hole effective mass, which comes from Ref. 15.

	InP	InAs
Gap (eV)	1.42	0.42
m_e^*	0.079	0.024
$m_{\rm hh}^*$	0.65	0.41
lattice constant (Å)	5.8696	6.0588

For the materials involved, we use the same parameters as in Ref. 3 and reprinted in Table I. With a static dielectric constant of 12.29 for the InP substrate,[10] the dimensionless parameter $U = 0.127$. To estimate $\mathcal{V}_e$ and $\mathcal{V}_h$, we use the lattice constant of InP and the band offsets obtained from fitting a simple envelope-function model[11] to the average of experimentally measured exciton binding energies in thin quantum wells. Photoluminescence (PL) measurements performed on thin InAs/InP quantum wells by Schneider and Wessels,[5] by Kobayashi and Kobayashi,[6] and by Leonelli *et al.*[3] are used to obtain the offsets. We take into account the fact that the measurements of Ref. 6 have been made at 77 K by using a smaller InP band gap to extract the binding energies from the reported values. Before fitting the two-band envelope function model[11] to the data, we substract from all the measurements a correlation energy estimated to be around -16 meV from a simple two-band effective tight-binding model. The latter is a simplified version of the effective bond-orbital model[12] in which we have included the electron-hole interaction. From the data for quantum wells of two to five monolayers, we obtain a heavy-hole band offset of 0.29 eV, taking into account the effect of strain on the InAs layer (the difference between the InP and InAs band gaps is taken as 0.95 eV).[3] This leaves a conduction band offset of 0.66 eV. Now, using the fact that the height of a monolayer in the zinc-blende structure is $a/2$ (growth along the [001] direction), the dimensionless parameters $\mathcal{V}_e$ and $\mathcal{V}_h$ are 0.209 and 0.0924, respectively.

Note that in the above discussion, we do not consider the measurements made on monolayer quantum wells since the variation between the reported values for the binding energy is quite large (from 70 meV to 140 meV).[3,5,6] Monolayer quantum wells are very delicate to make and nonuniformity is present to a certain extent in all samples. The experimental values come from PL measurements which are known to give the lowest energy states (highest binding energy states). It can be misleading to use these values if some interface

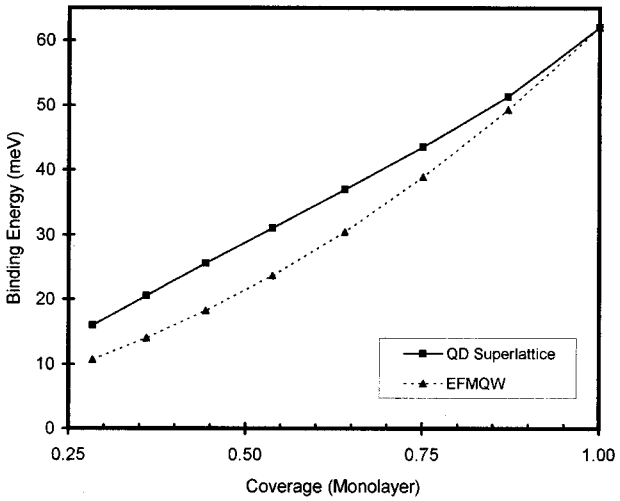

FIG. 2. Heavy-hole exciton binding energy for an InAs/InP QD superlattice with a 62.2 Å period as a function of the coverage. Values for an equivalent fractional monolayer quantum well (EFMQW) are also given.

roughness is present since one collects the signal from regions of largest thicknesses. This is exemplified in Ref. 3, where measurements from photoluminescence excitation spectroscopy (PLE) are also given. The latter technique is expected to give a more accurate picture of the distribution of energy states. For the monolayer quantum well (sample S4 of Ref. 3), the PLE measurement suggests a binding energy below 70 meV for the heavy-hole exciton while the PL measurement indicates an energy around 80 meV. Note that our model gives 62 meV when applied to the monolayer quantum-well structure, showing reasonable agreement with the PLE measurement.

In Figs. 2 and 3, we present, as a function of the coverage factor, the heavy-hole exciton binding energy and the magnitude of the correlation energy ($|E_{\mathrm{corr}}|$) for an InAs/InP QD

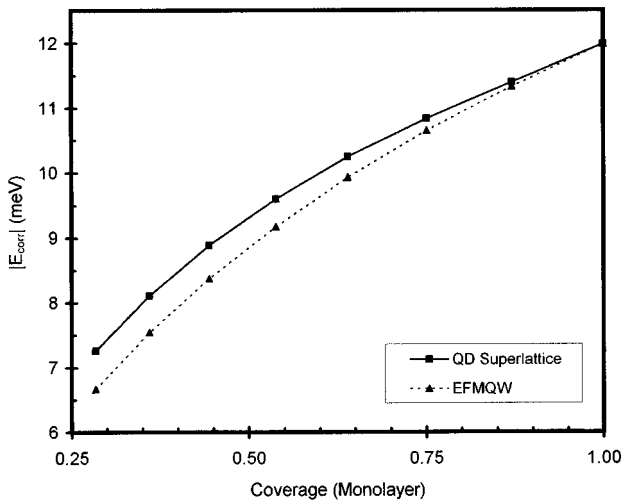

FIG. 3. Magnitude of the exciton correlation energy for an InAs/InP QD superlattice with a 62.2 Å period as a function of the coverage. Values for an equivalent fractional monolayer quantum well (EFMQW) are also given.

superlattice with a period of 62.2 Å. This period results from the growth of InAs quantum dots on an InP [001] surface tilted 2° towards [100]. This corresponds to the growth conditions of the QD superlattices studied in Ref. 3. For comparison, we also present values for an equivalent fractional monolayer quantum well (EFMQW) characterized by similar coverage factors. For this EFMQW, the InAs sites are distributed uniformly in the monolayer instead of being concentrated within quantum dots. The calculations for the EFMQW are performed with the same formalism as for a QD superlattice but with $L_p = L$ and with adjusted values of $\mathcal{V}_e$ and $\mathcal{V}_h$. We do not present results for coverage factors below 0.28: our model does not apply well to very low coverage factors since one cannot neglect the correlation induced along the growth direction by the Coulomb interaction.

For the calculated quantum-dot structures, the variational parameter $1/\alpha_{xy}$ is larger than the superlattice period. We have calculated the one-particle minibands using a generalization of the procedure presented in Sec. III. We have found that for all these structures, the superlattice effective mass of the exciton is close to that of InP and that the periodic part of the electron and hole one-particle Bloch states do not vary much over the Brillouin zones. Consequently, as discussed in Sec. II, we expect our variational treatment to give a good approximation for the binding energy.

The binding energy and the magnitude of the correlation energy increase with the coverage factor for both the QD superlattice and EFMQW cases. This increase is a consequence of the confinement introduced by the QD or EFMQW structures along the growth direction. This confinement is more pronounced for large coverage factors. The magnitude of the correlation energy varies monotonically starting from the InP bulk exciton value ($|E_{\mathrm{corr}}| \approx 6.3$ meV) for low coverage factors. For large coverage factors, the magnitude of the correlation energy remains smaller than the InP 2D exciton value ($|E_{\mathrm{corr}}| \approx 25.4$ meV) since the confinement introduced by a full monolayer of InAs is not strong enough to achieve a 2D exciton.

The binding energy is substantially higher in the QD superlattice case than in the EFMQW case. This increase is also observed for the magnitude of the correlation energy, but in a much smaller proportion. In fact, a careful study of the different contributions to the binding energy shows that most of the difference comes from the increase of the hole confinement energy ($|E_h|$). The superlattice potential modulates the one-particle wave functions in the x-y plane, increasing the probability of presence within the quantum dots. This modulation insures a better confinement effectiveness of the InAs sites in the QD superlattice case over the EFMQW case where such a modulation is not present.

In Ref. 3, measurements are given for samples with coverage factors of 0.3 and 0.8. For reasons previously discussed, the binding energies given by these PL measurements are not reliable enough to attempt a direct comparison with our calculations. However, the displacement of the PL peak indicates that the binding energy decreases by 34 meV when the nominal coverage factor is reduced by an amount of 0.5 (from 0.8 to 0.3). From the slope of the curve presented in Fig. 2, our calculations suggest a decrease of the order of 30 meV when the coverage factor is reduced by 0.5.

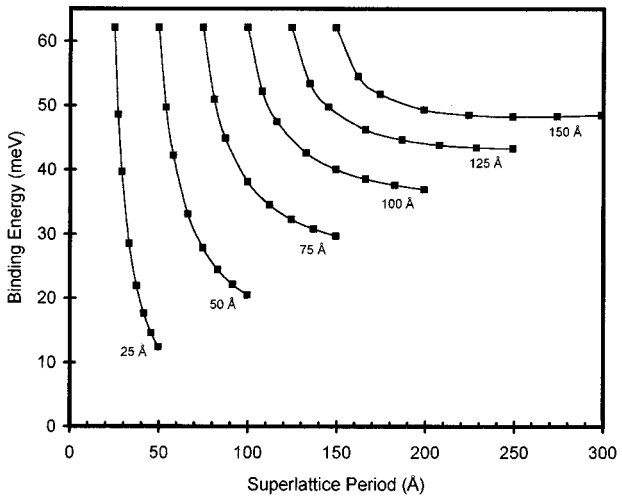

FIG. 4. Heavy-hole exciton binding energy for an InAs/InP QD superlattice for various QD dimensions as a function of the period of the superlattice.

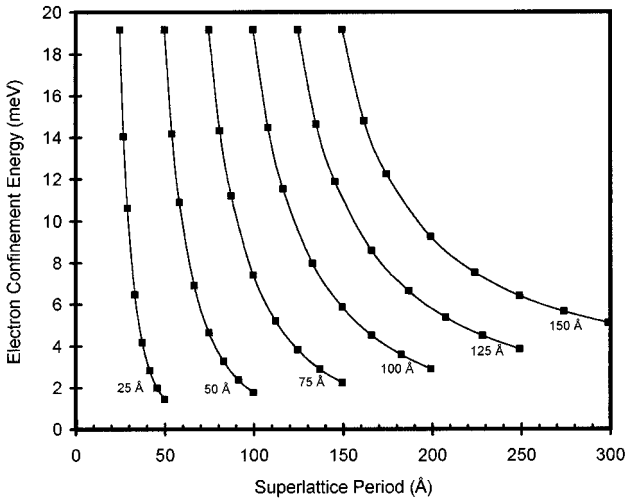

FIG. 6. Electron confinement energy for an InAs/InP QD superlattice for various QD dimensions as a function of the period of the superlattice.

The agreement is quite good considering the uncertainty about the exact nature of the QD superlattices studied in Ref. 3 and the uncertainty about the parameters used in our model, especially regarding the InP heavy-hole effective mass and the band offsets.

To give a better picture of the dependence of the heavy-hole exciton ground-state energy on the QD superlattice parameters, Fig. 4 presents the binding energy for various QD dimensions (25 Å, 50 Å, 75 Å, 100 Å, and 150 Å) (Ref. 13) as a function of the superlattice period. The corresponding hole and electron confinement energies are provided in Figs. 5 and 6. The magnitude of the correlation energy and the value of $1/\alpha_{xy}$ are also presented in Figs. 7 and 8, respectively. We have restricted our calculations to coverage factors larger than 0.25. The largest superlattice period of 300 Å corresponds to the growth of InAs quantum dots on an InP [001] surface tilted 0.4° towards [100].

For the smallest structures, the variational parameter $1/\alpha_{xy}$ is larger than the superlattice period, and a characterization of the minibands again shows that the criteria discussed in Sec. II are met. For the largest structures, the hole wave function is confined to the quantum dots while the electron wave function is strongly modulated. Those structures are close to the quantum-dot array limit also discussed in Sec. II and our variational treatment should again give a good approximation for the exciton binding energy. Between those limits, our treatment should provide some insight about the effect of the various parameters by giving an upper limit to the ground-state energy.

Figure 4 shows that the exciton binding energy varies considerably for small quantum dots as the superlattice period increases while the variation is much less pronounced for larger quantum dots. This can be related to the fact that the main contribution to the binding energy comes from the

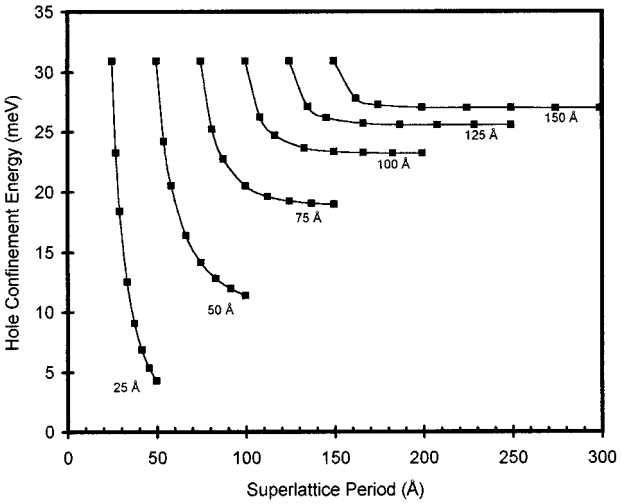

FIG. 5. Hole confinement energy for an InAs/InP QD superlattice for various QD dimensions as a function of the period of the superlattice.

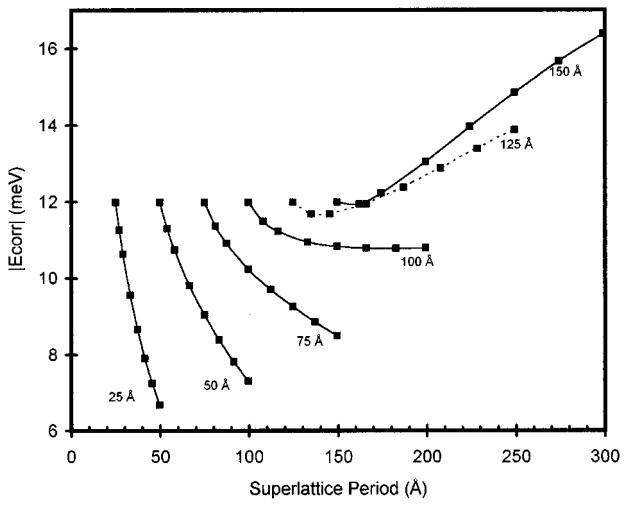

FIG. 7. Magnitude of the exciton correlation energy for an InAs/InP QD superlattice for various QD dimensions as a function of the period of the superlattice.

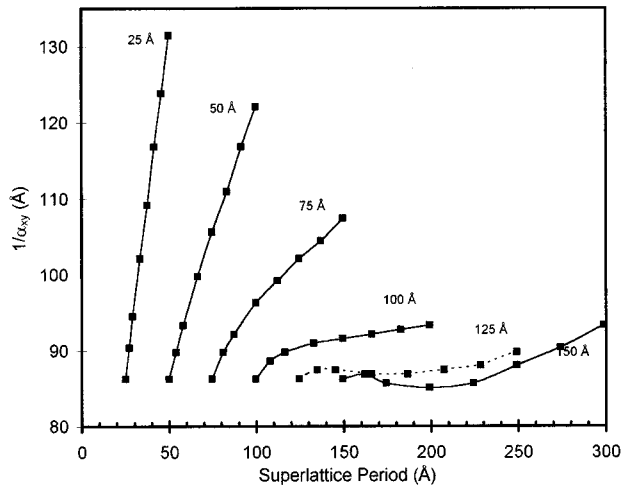

FIG. 8. Value of the variational parameter $1/\alpha_{xy}$ for an InAs/InP QD superlattice for various QD dimensions as a function of the period of the superlattice.

hole confinement energy. The hole wave function being well confined by the larger quantum dots, the corresponding hole confinement energy does not vary much with the superlattice period, as can be seen from Fig. 5. Figure 6 indicates that the electron confinement energy contribution is smaller and that it varies considerably with the superlattice period for all the QD dimensions considered, a consequence of the smaller electron effective mass. In fact, the electron confinement energy shows a dependence on the superlattice period that is similar to the hole confinement energy, but on a length scale about three times larger.

When the superlattice period increases, Fig. 7 indicates that the magnitude of the correlation energy decreases for quantum dots smaller than 100 Å. Since the electron wave function is less confined than the hole wave function, the former is mostly responsible for the behavior of the correlation energy. For small quantum dots, the electron wave function is weakly modulated in the x-y plane. The electron then interacts with an average potential in the superlattice plane and the extension of its wave function along the growth direction varies considerably with the superlattice period. As the superlattice period increases, the electron wave function becomes more spread out in the z direction, thus leading to a smaller electron-hole interaction. For quantum dots larger than 100 Å, the magnitude of the correlation energy increases with the superlattice period. The electron wave function is more strongly modulated in the x-y plane and its extension along the z direction is less dependent on the superlattice period. Consequently, as the superlattice period increases, the electron-hole interaction is enhanced since the electron wave function becomes more confined laterally to the quantum dot while its extension along the growth direction remains about the same. For superlattice periods larger than those considered in Fig. 7, the magnitude of the correlation energy reaches a maximum and then decreases slightly. For example, a detailed study of the 150 Å QD case shows that a maximum value of 18.5 meV is obtained for a superlattice period of about 500 Å.

Since the one-particle wave functions are weakly modulated in the x-y plane for small quantum dots, the value of $1/\alpha_{xy}$ presented in Fig. 8 can be used to obtain a good estimate of the extension of the exciton wave function. With the correlating function defined in Eq. (4), we find that the mean lateral separation between the electron and the hole in the superlattice plane $[\sqrt{\langle (x_e-x_h)^2+(y_e-y_h)^2\rangle}]$ is approximately given by $\sqrt{1.5}/\alpha_{xy}$. For a three-dimensional exciton in InP, this separation is given by $\sqrt{2}a^*_{\mathrm{InP}}$ where a^*_{InP} is the exciton Bohr radius (92 Å). Figure 8 thus indicates that, for small quantum dots, the lateral extension of the exciton wave function is slightly smaller than that of the three-dimensional exciton in InP. Note that our model overestimates $1/\alpha_{xy}$ for small coverage factors: this is a consequence of the neglect of the correlation induced by the Coulomb interaction along the growth direction (for small quantum dots with a coverage factor of 0.25, the error is of the order of 10%). For larger quantum dots, the value of $1/\alpha_{xy}$ indicates that the exciton does not spread over many quantum dots. This is clearly related to the increase of the electron-hole interaction previously discussed.

VI. CONCLUSION

In this paper, we have presented a simple two-band variational formalism for the characterization of the ground state of an exciton in a two-dimensional QD superlattice grown on a terraced substrate. The exciton wave function and the binding energy are obtained in a two-step process. First, the one-particle ground states of the superlattice are determined by numerically solving the Schrödinger equation in a QD superlattice for both the electron and hole. The exciton wave function and the binding energy are then obtained from a variational ansatz, the minimization process being performed numerically.

When applied to InAs/InP QD superlattices, our model predicts a decrease of the binding energy as the superlattice period increases. This variation is larger for small quantum dots. The electron-hole interaction has been found to decrease as the superlattice period increases for quantum dots smaller than 100 Å while it increases for larger quantum dots.

A strong variation of the binding energy with the QD dimensions has been experimentally observed for InAs/InP QD superlattices.[3] A fair agreement between our model and the available experimental measurements has been found for the variation of the exciton binding energy with the coverage factor. Since only a few samples have been produced and characterized up to now, there still remains a lot of uncertainty about the exact nature of the QD superlattices experimentally studied. Although the experimental work already performed on InAs/InP QD superlattices represents in itself quite an achievement, more work is needed to get a better knowledge of the shape, dimensions, and uniformity of the quantum dots resulting from the various growth conditions. For the optical characterization, more reliable binding energies would be obtained if photoluminescence studies could be complemented with PLE or absorption measurements. Only with this information could we further evaluate the validity of our model.

ACKNOWLEDGMENTS

This research has been supported by the Conseil de Recherches en Sciences Naturelles et en Génie du Canada (CRSNG) and by le Ministère de l'Éducation du Québec [le Fonds pour la Formation de Chercheurs et l'Aide à la Recherche (FCAR)]. We would also like to thank Dr. Richard Leonelli for numerous valuable discussions.

APPENDIX A

In this appendix, we provide more details for the derivation of the results of Sec. IV [Eqs. (17) and (18)]. These derivations are rather lengthy, so only the main steps are given.

For all the integrations over the electron and hole coordinates, we assume that the sample is infinite along the z direction and that the superlattice covers a large area A in the x-y plane. To obtain Eq. (17), we first use the following Fourier expansion:

$$F^2(\vec{r}_e,\vec{r}_h)=\frac{4\pi\alpha_{xy}}{A}\sum_{\vec{k}_{xy}}\frac{\exp[i\vec{k}_{xy}\cdot(\vec{r}_e-\vec{r}_h)]}{(4\alpha_{xy}^2+k_x^2+k_y^2)^{3/2}}, \tag{A1}$$

where the summation is performed over the two-dimensional wave-vector space of the QD superlattice. We can thus write

$$\int_V\int_V\psi_e(\vec{r}_e)^2\psi_h(\vec{r}_h)^2F(\vec{r}_e,\vec{r}_h)^2d^3r_ed^3r_h=\frac{4\pi\alpha_{xy}}{A}\sum_{\vec{k}_{xy}}\frac{1}{(4\alpha_{xy}^2+k_x^2+k_y^2)^{3/2}}\int_V\int_V\psi_e(\vec{r}_e)^2\psi_h(\vec{r}_h)^2$$
$$\times\exp[i\vec{k}_{xy}\cdot(\vec{r}_e-\vec{r}_h)]d^3r_ed^3r_h. \tag{A2}$$

To evaluate the remaining integrals, we first obtain

$$\int_V\psi_e(\vec{r}_e)^2\exp(i\vec{k}\cdot\vec{r}_e)d^3r_e=\frac{A}{8}\sum_{n_1\geqslant n_2,n_3\geqslant n_4}C_{e,n_1,n_2}C_{e,n_3,n_4}N_{n_1,n_2}N_{n_3,n_4}\frac{(\beta_{e,n_1,n_2}+\beta_{e,n_3,n_4})}{[k_z^2+(\beta_{e,n_1,n_2}+\beta_{e,n_3,n_4})^2]}\Delta_{n_1,n_2,n_3,n_4}(\vec{k}_{xy}), \tag{A3}$$

where $\Delta_{n_1,n_2,n_3,n_4}(\vec{k}_{xy})$ is defined by the following summation of products of Kronecker deltas:

$$\Delta_{n_1,n_2,n_3,n_4}(\vec{k}_{xy})=\sum_{i,j=1,2;i\neq j}\ \sum_{l,m=3,4;l\neq m}\ \sum_{s,t,u,v=\pm1}\delta\left(\frac{k_x}{q},sn_i+tn_l\right)\delta\left(\frac{k_y}{q},un_j+vn_m\right). \tag{A4}$$

An expression similar to Eq. (A3) is obtained from the integration over the hole coordinates in Eq. (A2). Note that the definition of $\Delta_{n_1,n_2,n_3,n_4}(\vec{k}_{xy})$ [Eq. (A4)] indicates that the summation over $\vec{k}_{xy}$ in Eq. (A2) can be restricted to the reciprocal lattice vectors of the QD superlattice. Finally, after introducing the electron and hole versions of Eq. (A3) into Eq. (A2), one can easily obtain Eq. (17) of Sec. IV, where the function $M_1(K_{xy})$ is given by

$$M_1(K_{xy})=\sum_{n_1\geqslant n_2,n_3\geqslant n_4,n_5\geqslant n_6,n_7\geqslant n_8}\frac{C_{e,n_1,n_2}C_{e,n_3,n_4}C_{h,n_5,n_6}C_{h,n_7,n_8}N_{n_1,n_2}N_{n_3,n_4}N_{n_5,n_6}N_{n_7,n_8}}{(\beta_{e,n_1,n_2}+\beta_{e,n_3,n_4})(\beta_{h,n_5,n_6}+\beta_{h,n_7,n_8})}$$
$$\times\sum_{\vec{k}_{xy};|\vec{k}_{xy}|=K_{xy}}\Delta_{n_1,n_2,n_3,n_4}(\vec{k}_{xy})\Delta_{n_5,n_6,n_7,n_8}(\vec{k}_{xy}). \tag{A5}$$

The derivation Eq. (18) is done along similar lines. It starts with the following Fourier expansion:

$$\frac{F^2(\vec{r}_e,\vec{r}_h)}{|\vec{r}_e-\vec{r}_h|}=\frac{2}{A}\sum_{\vec{k}_{xy}}\int_{-\infty}^{+\infty}\left[\int_0^\infty\exp(-2\alpha_{xy}\rho)\rho J_0(k_{xy}\rho)\int_0^\infty\frac{\cos(k_zw)}{\sqrt{\rho^2+w^2}}dwd\rho\right]\exp[i\vec{k}\cdot(\vec{r}_e-\vec{r}_h)]dk_z, \tag{A6}$$

where $J_0(k_{xy}\rho)$ is the zeroth order Bessel function.[8] Introducing this expression into the left side of Eq. (18) and using the electron and hole versions of Eq. (A3), one obtains the right side of Eq. (18) after a simple integration over the k_z variable. The function $M_2(K_{xy},w)$ of Eq. (18) is defined by

$$M_2(K_{xy},w)=\sum_{n_1\geqslant n_2,n_3\geqslant n_4,n_5\geqslant n_6,n_7\geqslant n_8}\frac{C_{e,n_1,n_2}C_{e,n_3,n_4}C_{h,n_5,n_6}C_{h,n_7,n_8}N_{n_1,n_2}N_{n_3,n_4}N_{n_5,n_6}N_{n_7,n_8}}{[(\beta_{h,n_5,n_6}+\beta_{h,n_7,n_8})^2-(\beta_{e,n_1,n_2}+\beta_{e,n_3,n_4})^2]}$$
$$\times\{\exp[-(\beta_{e,n_1,n_2}+\beta_{e,n_3,n_4})w](\beta_{h,n_5,n_6}+\beta_{h,n_7,n_8})$$
$$-\exp[-(\beta_{h,n_5,n_6}+\beta_{h,n_7,n_8})w](\beta_{e,n_1,n_2}+\beta_{e,n_3,n_4})\}\sum_{\vec{k}_{xy};|\vec{k}_{xy}|=K_{xy}}\Delta_{n_1,n_2,n_3,n_4}(\vec{k}_{xy})\Delta_{n_5,n_6,n_7,n_8}(\vec{k}_{xy}). \quad \text{(A7)}$$

[1] O. Brandt, L. Tapfer, K. Ploog, R. Bierwolf, M. Hohenstein, F. Phillip, H. Lage, and A. Heberle, Phys. Rev. B **44**, 8043 (1991).

[2] C.A. Tran, R.A. Masut, J.L. Brebner, R. Leonelli, J.T. Graham, and P. Cova, J. Cryst. Growth **124**, 596 (1992).

[3] R. Leonelli, C.A. Tran, J.L. Brebner, J.T. Graham, R. Tabti, R.A. Masut, and S. Charbonneau, Phys. Rev. B **48**, 11 135 (1993).

[4] R. Cingolani, O. Brandt, L. Tapfer, G. Scamarcio, G.C. La Rocca, and K. Ploog, Phys. Rev. B **42**, 3209 (1990).

[5] R.P. Schneider, Jr. and B.W. Wessels, J. Appl. Phys. **70**, 405 (1991).

[6] N. Kobayashi and Y. Kobayashi, J. Cryst. Growth **124**, 525 (1992).

[7] L. Bányai and S.W. Koch, *Semiconductor Quantum Dots* (World Scientific, Singapore, 1993).

[8] I.S. Gradshteyn and I.M. Ryzhik, *Table of Integrals, Series and Products* (Academic Press, New York, 1980).

[9] S. Le Goff and B. Stébé, Phys. Rev. B **47**, 1383 (1993).

[10] E. Kartheuser, in *Polarons in Ionic Crystals and Polar Semiconductors*, edited by J.T. Devreese (North-Holland, Amsterdam, 1972), p. 717.

[11] G. Bastard, *Wave Mechanics Applied to Semiconductor Heterostructures* (Les Editions de Physique, Paris, 1988).

[12] Y.-C. Chang, Phys. Rev. B **37**, 8215 (1988).

[13] The true QD dimensions used in the calculations are multiples of $a/\sqrt{2}$, where a is the InP lattice constant. Consequently, the dimensions that we have considered are 24.9 Å, 49.8 Å, 74.7 Å, 99.6 Å, 124.5 Å, and 149.4 Å. For simplicity, we refer to them in the text as 25 Å, 50 Å, 75 Å, 100 Å, 125 Å, and 150 Å, respectively.

[14] *Numerical Data and Functional Relationships in Science and Technology*, edited by O. Madelung, M. Schulz, and H. Weiss, Landolt-Börnstein, New Series III/17a (Springer-Verlag, Berlin, 1982).

[15] J.D. Wiley, in *Semiconductors and Semimetals*, edited by R.K. Willardson and A.C. Beers (Academic Press, New York, 1975), Vol. 10, p. 91.